Supplemental Material: Theory of Subcycle Linear Momentum Transfer in Strong-Field Tunneling Ionization

Hongcheng Ni,[1,2] Simon Brennecke,[3] Xiang Gao,[2] Pei-Lun He,[4] Stefan Donsa,[2] Iva Březinová,[2] Feng He,[4] Jian Wu,[1] Manfred Lein,[3] Xiao-Min Tong,[5] and Joachim Burgdörfer[2]

[1]*State Key Laboratory of Precision Spectroscopy, East China Normal University, Shanghai 200241, China*
[2]*Institute for Theoretical Physics, Vienna University of Technology, 1040 Vienna, Austria, EU*
[3]*Institut für Theoretische Physik, Leibniz Universität Hannover, 30167 Hannover, Germany, EU*
[4]*Key Laboratory for Laser Plasmas (Ministry of Education) and School of Physics and Astronomy, Collaborative Innovation Center for IFSA (CICIFSA), Shanghai Jiao Tong University, Shanghai 200240, China*
[5]*Center for Computational Sciences, University of Tsukuba, Tsukuba, Ibaraki 305-8573, Japan*

S1. BACKPROPAGATION IN THE NONDIPOLE REGIME

In order to extract accurate information on the momentum distribution of ionized electrons at the tunnel exit, we extend the backpropagation method [1–3] to the nondipole regime. The method involves two steps: We first propagate the quantum wave packet forward in time until an ensemble of virtual detectors is reached. In the second step, semiclassical trajectories are propagated backward in time until the tunnel exit is reached. To initiate the backpropagation, the outgoing flux needs to be converted into classical trajectories when the laser field is still on. To this end, we need to find the appropriate flux associated with the Hamiltonian. The time-dependent Schrödinger equation can be written as

$$i\frac{\partial}{\partial t}\psi = \left\{\frac{1}{2}\left[\boldsymbol{p}+\boldsymbol{A}(t)+\frac{\boldsymbol{e}_z}{c}\left(\boldsymbol{p}\cdot\boldsymbol{A}(t)+\frac{1}{2}A^2(t)\right)\right]^2 + V\left(\boldsymbol{r}-\frac{z}{c}\boldsymbol{A}(t)\right)\right\}\psi, \tag{S1}$$

the conjugate of which is

$$-i\frac{\partial}{\partial t}\psi^* = \left\{\frac{1}{2}\left[-\boldsymbol{p}+\boldsymbol{A}(t)+\frac{\boldsymbol{e}_z}{c}\left(-\boldsymbol{p}\cdot\boldsymbol{A}(t)+\frac{1}{2}A^2(t)\right)\right]^2 + V\left(\boldsymbol{r}-\frac{z}{c}\boldsymbol{A}(t)\right)\right\}\psi^*. \tag{S2}$$

Multiplying Eq. (S1) by ψ^* from the left, multiplying Eq. (S2) by ψ from the left, and doing the subtraction, we have

$$\begin{aligned} i\frac{\partial}{\partial t}|\psi|^2 =& \frac{1}{2}\psi^*\left[\boldsymbol{p}+\boldsymbol{A}(t)+\frac{\boldsymbol{e}_z}{c}\left(\boldsymbol{p}\cdot\boldsymbol{A}(t)+\frac{1}{2}A^2(t)\right)\right]^2\psi - \frac{1}{2}\psi\left[-\boldsymbol{p}+\boldsymbol{A}(t)+\frac{\boldsymbol{e}_z}{c}\left(-\boldsymbol{p}\cdot\boldsymbol{A}(t)+\frac{1}{2}A^2(t)\right)\right]^2\psi^* \\ =& -i\boldsymbol{\nabla}\cdot\left\{\frac{1}{2}(\psi^*\boldsymbol{p}\psi-\psi\boldsymbol{p}\psi^*)+\boldsymbol{A}\left[|\psi|^2+\frac{1}{2c}(\psi^*p_z\psi-\psi p_z\psi^*)+\frac{1}{2c^2}(\psi^*\boldsymbol{p}\cdot\boldsymbol{A}\psi-\psi\boldsymbol{p}\cdot\boldsymbol{A}\psi^*)+\frac{A^2}{2c^2}|\psi|^2\right]\right. \\ &\left.+\frac{\boldsymbol{e}_z}{2c}(\psi^*\boldsymbol{p}\cdot\boldsymbol{A}\psi-\psi\boldsymbol{p}\cdot\boldsymbol{A}\psi^*)+\frac{\boldsymbol{e}_z}{2c}A^2|\psi|^2\right\}. \end{aligned} \tag{S3}$$

According to the equation of continuity $\frac{\partial}{\partial t}\rho+\boldsymbol{\nabla}\cdot\boldsymbol{j}=0$, where $\rho\equiv|\psi|^2$, the probability flux $\boldsymbol{j}$ is given by

$$\begin{aligned} \boldsymbol{j} =& \frac{1}{2}(\psi^*\boldsymbol{p}\psi-\psi\boldsymbol{p}\psi^*)+\boldsymbol{A}\left[|\psi|^2+\frac{1}{2c}(\psi^*p_z\psi-\psi p_z\psi^*)+\frac{1}{2c^2}(\psi^*\boldsymbol{p}\cdot\boldsymbol{A}\psi-\psi\boldsymbol{p}\cdot\boldsymbol{A}\psi^*)+\frac{A^2}{2c^2}|\psi|^2\right] \\ &+\frac{\boldsymbol{e}_z}{2c}(\psi^*\boldsymbol{p}\cdot\boldsymbol{A}\psi-\psi\boldsymbol{p}\cdot\boldsymbol{A}\psi^*)+\frac{\boldsymbol{e}_z}{2c}A^2|\psi|^2. \end{aligned} \tag{S4}$$

If we write the wavefunction in "polar" form as $\psi=\sqrt{\rho}e^{iS}$, we find

$$\boldsymbol{j} = \rho\boldsymbol{\nabla}S+\rho\boldsymbol{A}\left\{1+\frac{1}{c}\left[\frac{\partial S}{\partial z}+\frac{1}{c}\left(\boldsymbol{\nabla}S\cdot\boldsymbol{A}+\frac{1}{2}A^2\right)\right]\right\}+\rho\frac{\boldsymbol{e}_z}{c}\left(\boldsymbol{\nabla}S\cdot\boldsymbol{A}+\frac{1}{2}A^2\right). \tag{S5}$$

Expressing the current density as $\boldsymbol{j}=\rho\boldsymbol{v}$, we obtain the local velocity $\boldsymbol{v}$ during the pulse

$$\boldsymbol{v} = \boldsymbol{\nabla}S+\boldsymbol{A}\left\{1+\frac{1}{c}\left[\frac{\partial S}{\partial z}+\frac{1}{c}\left(\boldsymbol{\nabla}S\cdot\boldsymbol{A}+\frac{1}{2}A^2\right)\right]\right\}+\frac{\boldsymbol{e}_z}{c}\left(\boldsymbol{\nabla}S\cdot\boldsymbol{A}+\frac{1}{2}A^2\right). \tag{S6}$$

Note that the Hamiltonian we use adds a "shear" to the atomic potential, effectively changing the velocity defined in this frame as compared to the lab frame. In order to obtain the observables in the lab frame, the following frame transform is required:

$$\boldsymbol{r}_{\rm lab} = \boldsymbol{r}-z\boldsymbol{A}/c, \tag{S7}$$

$$\boldsymbol{v}_{\rm lab} = \boldsymbol{v}+z\boldsymbol{F}/c-v_z\boldsymbol{A}/c. \tag{S8}$$

S2. THE GENERALIZED PSEUDOSPECTRAL METHOD FOR NONDIPOLE THREE-DIMENSIONAL TDSE

The Hamiltonian used in the main text [Eq. (2)] is presented in a "sheared" gauge to facilitate TDSE simulations with the Fourier method. To check the numerical convergence of the Fourier method, we also developed the generalized pseudospectral method to solve the three-dimensional TDSE beyond the dipole approximation using a length-gauge Hamiltonian with nondipole corrections to order $1/c$:

$$H_L = \left[\frac{1}{2}\tilde{\boldsymbol{p}}^2 + V(r)\right] + \boldsymbol{r}\cdot\boldsymbol{F}(t) + \frac{z}{c}\tilde{\boldsymbol{p}}\cdot\boldsymbol{F}(t) = H_0 + H_1 + H_2, \tag{S9}$$

with $H_0 = \tilde{\boldsymbol{p}}^2/2 + V(r)$, $H_1 = \boldsymbol{r}\cdot\boldsymbol{F}(t)$, and $H_2 = \frac{z}{c}\tilde{\boldsymbol{p}}\cdot\boldsymbol{F}(t)$, where $\tilde{\boldsymbol{p}}$ is the corresponding canonical momentum. The part $H_0 + H_1$ is the Hamiltonian in dipole approximation in length gauge, and can be readily solved by the time propagator based on the second-order split-operator method [4] and the generalized pseudospectral method [5–7]. With the use of a Taylor expansion for the time propagator of the H_2 term, we can perform numerical simulations with the Hamiltonian H_L in a similar framework. More specifically, the time propagator for H_L can be expressed as

$$U(t+\Delta t) = \exp(-iH_0\Delta t/2)\exp(-iH_1\Delta t/2)\exp(-iH_2\Delta t)\exp(-iH_1\Delta t/2)\exp(-iH_0\Delta t/2). \tag{S10}$$

The propagation of $\exp(-iH_0\Delta t/2)$ is done in energy space, and $\exp(-iH_1\Delta t/2)$ is evaluated in position space. Afterwards, we continue evaluating the $\exp(-iH_2\Delta t)$ part in position space using a Taylor expansion

$$\exp\left(-iH_2\Delta t\right) \approx \sum_{n=0}^{n_{\max}} \frac{(-iH_2\Delta t)^n}{n!}. \tag{S11}$$

For the system considered in the present work, we found $n_{\max} = 8$ for each time step is adequate to obtain converged results. The momentum distribution is obtained using the same technique as in [8], except that the Volkov propagator applied to the absorbed wave packet at each time step is substituted with the nondipole version, which is calculated numerically with a similar procedure.

S3. NONDIPOLE STRONG-FIELD APPROXIMATION

The nondipole strong-field approximation (SFA) offers the possibility to model recollision-free strong-field ionization without the computational demanding solution of the exact time-dependent Schrödinger equation. For the calculations, we use the Hamiltonian in length gauge, H_L [Eq. (S9)], neglecting, however, the atomic potential in H_0,

$$H_L = \frac{1}{2}\tilde{\boldsymbol{p}}^2 + \boldsymbol{r}\cdot\boldsymbol{F}(t) + \frac{z}{c}\tilde{\boldsymbol{p}}\cdot\boldsymbol{F}(t). \tag{S12}$$

The initial kinetic momentum (or velocity in a.u.) at the tunnel exit $\boldsymbol{v}$ relates to the asymptotic momentum $\boldsymbol{p}$ as

$$\boldsymbol{v} = \boldsymbol{p} + \boldsymbol{A} + \frac{\boldsymbol{e}_z}{2c}[(\boldsymbol{p}+\boldsymbol{A})^2 - p^2] = \boldsymbol{p} + \boldsymbol{A} + \frac{\boldsymbol{e}_z}{2c}(v_\perp^2 - p_\perp^2). \tag{S13}$$

In the modified SFA evaluated in the saddle-point approximation, the transition rate is calculated from [9–11]

$$W_{\text{ndSFA}} = |\ddot{S}|^{-\alpha_Z}\exp\{2\text{Im}S\}, \tag{S14}$$

where $\alpha_Z = 1 + Z/\sqrt{2I_p}$ with Z the asymptotic charge of the remaining ion. For a short-range potential, $\alpha_Z = \alpha_0 = 1$. In the nondipole version of SFA (ndSFA), the action including nondipole corrections to the order $1/c$ can be expressed as [12]

$$S = \int_{t_s}^{t_r}\left\{\frac{1}{2}\left[\boldsymbol{p} + \boldsymbol{A}(t) + \frac{\boldsymbol{e}_z}{c}\left(\boldsymbol{p}\cdot\boldsymbol{A}(t) + \frac{1}{2}A^2(t)\right)\right]^2 + I_p\right\}dt. \tag{S15}$$

The saddle point is given by

$$\frac{1}{2}\left[\boldsymbol{p} + \boldsymbol{A}(t_s) + \frac{\boldsymbol{e}_z}{c}\left(\boldsymbol{p}\cdot\boldsymbol{A}(t_s) + \frac{1}{2}A^2(t_s)\right)\right]^2 + I_p = 0, \tag{S16}$$

where the saddle-point time $t_s = t_r + it_i$ must be complex in order to solve Eq. (S16). After solving the saddle-point equation (S16) the photoelectron momentum distribution can be calculated directly by evaluating Eq. (S14). Reduced quantities such

as the ionization probability P_I as a function of the attoclock angle ϕ_p, as shown in Fig. 3(b) of the main text, follow from integration over the remaining variables. However, in order to calculate observables as a function of the release time t_r we have to integrate over all momenta that belong to this given real part of the saddle-point time. To this end, it is advantageous to perform a coordinate transformation $(p_x, p_y, p_z) \to (t_r, k_\perp, p_z)$ with the release time t_r chosen as the real part of the saddle-point time t_s, the momentum component in the polarization plane

$$k_\perp = (\boldsymbol{p} + \mathrm{Re}\boldsymbol{A}(t_s)) \cdot (\mathrm{Im}A_y(t_s)\boldsymbol{e}_x - \mathrm{Im}A_x(t_s)\boldsymbol{e}_y) \,/\, \sqrt{(\mathrm{Im}A_x(t_s))^2 + (\mathrm{Im}A_y(t_s))^2} \tag{S17}$$

and the z-component of the final momentum p_z. The probability density in these variables is accordingly given by

$$\tilde{w}(t_r, k_\perp, p_z) = \left| \det \frac{\partial(p_x, p_y, p_z)}{\partial(t_r, k_\perp, p_z)} \right| W_{\mathrm{ndSFA}}(\boldsymbol{p}). \tag{S18}$$

The subcycle time-resolved linear momentum transfer shown in Fig. 2 of the main text can now be obtained as the average of the initial velocity in the light propagation direction

$$\langle v_z(t_r) \rangle = \frac{\int \mathrm{d}k_\perp \mathrm{d}p_z \, v_z(t_r, k_\perp, p_z) \, \tilde{w}(t_r, k_\perp, p_z)}{\int \mathrm{d}k_\perp \mathrm{d}p_z \, \tilde{w}(t_r, k_\perp, p_z)}. \tag{S19}$$

Expansion of the vector potential $\boldsymbol{A}(t_r + it_i)$ in powers of t_i [3, 13–16],

$$\boldsymbol{A}(t_r + it_i) = \boldsymbol{A}(t_r) - it_i \boldsymbol{F}(t_r) + \frac{1}{2} t_i^2 \dot{\boldsymbol{F}}(t_r) + O(t_i^3), \tag{S20}$$

allows to simplify the ndSFA and to gain additional insights. Inserting into Eq. (S16) and keeping the terms up to the second order in t_i results in

$$\boldsymbol{v}(t_r) \cdot \boldsymbol{F}(t_r) = 0, \tag{S21}$$

which is the termination criterion we use for the backpropagating trajectories, and

$$t_i = \sqrt{\frac{p^2 + \left(1 + \frac{p_z}{c}\right)\left[2\boldsymbol{p} \cdot \boldsymbol{A}(t_r) + A^2(t_r)\right] + 2I_p}{\left(1 + \frac{p_z}{c}\right)\left[F^2(t_r) - \boldsymbol{v}(t_r) \cdot \dot{\boldsymbol{F}}(t_r)\right]}}. \tag{S22}$$

The ionization rate [Eq. (S14)] depends exponentially on the argument

$$\begin{aligned} \mathrm{Im}S &= -I_p t_i - \frac{1}{2}\mathrm{Re}\int_0^{t_i} \left[\boldsymbol{p} + \boldsymbol{A}(t_r + it) + \frac{\boldsymbol{e}_z}{c}\left(\boldsymbol{p} \cdot \boldsymbol{A}(t_r + it) + \frac{1}{2}A^2(t_r + it)\right)\right]^2 dt \\ &\approx -\frac{\left[p^2 + \left(1 + \frac{p_z}{c}\right)\left(2\boldsymbol{p} \cdot \boldsymbol{A}(t_r) + A^2(t_r)\right) + 2I_p\right]^{3/2}}{3\sqrt{\left(1 + \frac{p_z}{c}\right)}\widetilde{F}(t_r)}, \end{aligned} \tag{S23}$$

with an effective field $\widetilde{F}(t_r) = \sqrt{F^2(t_r) - \boldsymbol{v}_\perp(t_r) \cdot \dot{\boldsymbol{F}}(t_r)}$ and on the nonexponential prefactor

$$\begin{aligned} |\ddot{S}|^{-\alpha_Z} &\approx |-i(1 + p_z/c)t_i \widetilde{F}^2|^{-\alpha_Z} \\ &\approx \left[\left(1 + \frac{p_z}{c}\right)\left(v_\perp^2 + p_z^2 + 2\frac{p_z}{c}\left(\boldsymbol{p} \cdot \boldsymbol{A} + \frac{A^2}{2}\right) + 2I_p\right)\widetilde{F}^2\right]^{-\alpha_Z/2}. \end{aligned} \tag{S24}$$

Eq. (S23) can be further simplified

$$\begin{aligned} \mathrm{Im}S &\approx -\frac{\left[v_\perp^2 + p_z^2 + \frac{p_z}{c}\left(v_\perp^2 - p_\perp^2\right) + 2I_p\right]^{3/2}}{3\sqrt{\left(1 + \frac{p_z}{c}\right)}\widetilde{F}} \\ &\approx -\frac{\left\{\left(1 - \frac{p_z}{3c}\right)\left[v_\perp^2 + p_z^2 + \frac{p_z}{c}\left(v_\perp^2 - p_\perp^2\right) + 2I_p\right]\right\}^{3/2}}{3\widetilde{F}} \\ &\approx -\frac{1}{3\widetilde{F}}\left[v_\perp^2 + \left(p_z - \left(\frac{p_\perp^2 - v_\perp^2}{2c} + \frac{2I_p + v_\perp^2}{6c}\right)\right)^2 + 2I_p\right]^{3/2}, \end{aligned} \tag{S25}$$

while Eq. (S24) can be accordingly approximated by

$$|\ddot{S}|^{-\alpha_Z} \approx \left[\left(v_\perp^2+2I_p\right)\widetilde{F}^2\right]^{-\alpha_Z/2}\left(1+\frac{p_z}{c}\right)^{-\alpha_Z/2}\left[1+\frac{p_z^2+2\frac{p_z}{c}\left(\boldsymbol{p}\cdot\boldsymbol{A}+\frac{A^2}{2}\right)}{v_\perp^2+2I_p}\right]^{-\alpha_Z/2}$$
$$\approx \left[\left(v_\perp^2+2I_p\right)\widetilde{F}^2\right]^{-\alpha_Z/2}\exp\left\{-\frac{\alpha_Z}{2}\frac{p_z}{c}\right\}\exp\left\{-\frac{\alpha_Z}{2}\frac{\left(p_z-\frac{p_\perp^2-v_\perp^2}{2c}\right)^2}{v_\perp^2+2I_p}\right\}. \tag{S26}$$

Hence, we arrive at

$$W_{\mathrm{ndSFA}} \approx \left[\left(v_\perp^2+2I_p\right)\widetilde{F}^2\right]^{-\alpha_Z/2}\exp\left\{-\frac{\alpha_Z}{2}\frac{p_z}{c}-\frac{\alpha_Z}{2}\frac{\left(p_z-\frac{p_\perp^2-v_\perp^2}{2c}\right)^2}{v_\perp^2+2I_p}-\frac{2}{3\widetilde{F}}\left[v_\perp^2+\left(p_z-\left(\frac{p_\perp^2-v_\perp^2}{2c}+\frac{2I_p+v_\perp^2}{6c}\right)\right)^2+2I_p\right]^{3/2}\right\}$$
$$\approx \left[\left(v_\perp^2+2I_p\right)\widetilde{F}^2\right]^{-\alpha_Z/2}\exp\left\{-\frac{2}{3\widetilde{F}}\left[v_\perp^2+\left(1+\frac{\alpha_Z\widetilde{F}}{2(v_\perp^2+2I_p)^{3/2}}\right)\left(p_z-\left(\frac{p_\perp^2-v_\perp^2}{2c}+\langle v_z(t_r,v_\perp)\rangle\right)\right)^2+2I_p\right]^{3/2}\right\}. \tag{S27}$$

The Jacobian in Eq. (S18) reads after the expansion of the vector potential in t_i (S20)

$$\left|\det\frac{\partial(p_x,p_y,p_z)}{\partial(t_r,k_\perp,p_z)}\right| \approx \left|\frac{v_\perp\left[F_x(t_r)F_y'(t_r)-F_x'(t_r)F_y(t_r)\right]}{F^2(t_r)}+F(t_r)\right|. \tag{S28}$$

To this order, it does not depend on p_z and, thus, has no influence in the transfer of longitudinal momentum. We therefore neglect this factor in the following.

In Eq. (S27), we introduce the partial average $\langle v_z(t_r,v_\perp)\rangle$ that is obtained by integration over p_z for fixed release time t_r and the perpendicular component of the velocity $v_\perp$

$$\langle v_z(t_r,v_\perp)\rangle = \frac{2I_p+v_\perp^2}{6c}\left[1-\frac{2\alpha_Z\widetilde{F}}{(2I_p+v_\perp^2)^{3/2}}\right] \approx \frac{2I_p+v_\perp^2}{6c}\left[1-\frac{2\alpha_Z F}{(2I_p)^{3/2}}\right], \tag{S29}$$

with the corresponding asymptotic linear momentum

$$\langle p_z(t_r,v_\perp)\rangle = \frac{p_\perp^2-v_\perp^2}{2c}+\langle v_z(t_r,v_\perp)\rangle. \tag{S30}$$

When focusing on the temporal dynamics only, one can additionally average over the perpendicular velocity $v_\perp$ and hence obtain for a fixed release time t_r the average linear momentum transfer at the tunnel exit $\langle v_z(t_r)\rangle$.

The effective field $\widetilde{F}=\sqrt{F^2-\boldsymbol{v}_\perp\cdot\dot{\boldsymbol{F}}}$ including the time derivative of the field, $\dot{\boldsymbol{F}}$, accounts for nonadiabatic effects. Consequently, $v_\perp$ is centered at nonzero values in Eqs. (S29) and (S30). Approximating the nonadiabatic correction to the lowest order in $\dot{\boldsymbol{F}}$ in the exponent

$$W_{\mathrm{ndSFA}} \approx \left[\left(v_\perp^2+2I_p\right)\widetilde{F}^2\right]^{-\alpha_Z/2}\exp\left\{-\frac{2}{3F}\left[\left(v_\perp^2+2I_p\right)\left(1+\frac{\boldsymbol{v}_\perp\cdot\dot{\boldsymbol{F}}}{3F^2}\right)\right]^{3/2}\right\}, \tag{S31}$$

where the first-order term in $\boldsymbol{v}_\perp$ shifts the center of the $v_\perp$ distribution from zero to a finite value. To obtain an explicit value, we have also neglected the momentum in the laser propagation direction, which would provide only a minimal contribution to the shift in $v_\perp$. Inserting the explicit expression for the laser field and assuming a flat envelope of the pulse yields

$$\langle v_\perp(t_r)\rangle \approx \frac{\varepsilon I_p}{3A_0\hat{F}(t_r)^3} \quad \text{with} \quad \hat{F}(t_r)=\sqrt{\cos^2(\omega t_r+\phi_{\mathrm{CEP}})+\varepsilon^2\sin^2(\omega t_r+\phi_{\mathrm{CEP}})}, \tag{S32}$$

which closely resembles the result of the Perelomov–Popov–Terent'ev (PPT) theory [17–23]. This nonadiabatic effect generates a subcycle modulation of the center of $v_\perp$ as well as $v_\perp^2$, which further results in a subcycle nonadiabatic modulation of the nondipole effect in Eq. (S31). If we approximate Eq. (S31) with a Gaussian distribution in $v_\perp$, it is easy to show that

$$\langle v_\perp^2(t_r)\rangle \approx \langle v_\perp(t_r)\rangle^2+\frac{F(t_r)}{2\sqrt{2I_p}}. \tag{S33}$$

Distinct contributions to the linear momentum at the tunnel exit [Eq. (S29)] can be studied at different levels of approximation. If we ignore the contribution from the nonexponential prefactor ($\alpha_Z = 0$),

$$\langle v_z(t_r)\rangle \approx \frac{2I_p + \langle v_\perp^2(t_r)\rangle}{6c} \approx \frac{I_p}{3c} + \frac{\varepsilon^2 I_p^2}{54cA_0^2\hat{F}^6(t_r)} + \frac{F_0\hat{F}(t_r)}{12c\sqrt{2I_p}}. \tag{S34}$$

For $\varepsilon \lesssim 1$ as in a typical attoclock setup, Eq. (S34) can be further approximated by

$$\langle v_z\rangle \approx \frac{I_p}{3c} + \frac{1}{12c}\left[\frac{\varepsilon^2 I_p^2}{9A_0^2}\left(1-\varepsilon^{-6}\right) + \frac{F_0}{2\sqrt{2I_p}}(1-\varepsilon)\right]\cos(2\omega t_r + 2\phi_{\mathrm{CEP}}) + \frac{1}{12c}\left[\frac{\varepsilon^2 I_p^2}{9A_0^2}\left(1+\varepsilon^{-6}\right) + \frac{F_0}{2\sqrt{2I_p}}(1+\varepsilon)\right]. \tag{S35}$$

Obviously, the nonadiabaticity of strong-field tunneling ionization introduces a 2ω subcycle modulation of the nondipole transfer of photon momentum at the tunnel exit, in agreement with what is found in the main text. Note that for the present laser parameters $\frac{\varepsilon^2 I_p^2}{9A_0^2}\left(1-\varepsilon^{-6}\right) + \frac{F_0}{2\sqrt{2I_p}}(1-\varepsilon) < 0$, hence the modulation phase agrees with that presented in the main text as well. The temporal average of $\langle v_z(t_r)\rangle$, however, is larger than $I_p/3c$. The inclusion of the prefactor with $\alpha_Z > 0$ generates the downward shift in qualitative agreement with the results determined by the backpropagation method (black dashed line in Fig. 2 of the main text).

Nonadiabatic tunneling effects may leave their mark on the experimentally observable asymptotic linear momentum transfer $\langle p_z\rangle$. From Eq. (S30), it is easy to show

$$\langle p_z(t_r)\rangle = A^2(t_r)/2c - \langle \boldsymbol{v}_\perp(t_r)\rangle \cdot \boldsymbol{A}(t_r)/c + \langle v_z(t_r)\rangle. \tag{S36}$$

Interestingly, the nonadiabaticity-induced subcycle variation in $\langle v_\perp(t_r)\rangle$ not only leads to modulations of the linear momentum transfer at the tunnel exit but also is amplified in $\langle p_z\rangle$ by its coupling to the vector potential. Provided the linear momentum resolution suffices, a decomposition of different contributions to the angular variation shown in Fig. 3 of the main text could indeed be pursued. It may even be possible to isolate the contribution of $\langle v_z(t_r)\rangle$ by removing the contribution of $\langle \boldsymbol{v}_\perp(t_r)\rangle \cdot \boldsymbol{A}(t_r)/c$ using, e.g., a standard SFA theory. For extracting $\langle v_z(t_r)\rangle$ from $\langle p_z(\phi_p)\rangle$ (Fig. S1), we transform the angular dependence of the asymptotic linear momentum transfer $\langle p_z(\phi_p)\rangle$ to the time axis using the linear mapping between time and angle in the elliptical coordinate [24] and obtain $\langle p_z(t_r)\rangle$ for the central cycle (blue line), from which different contributions can be isolated.

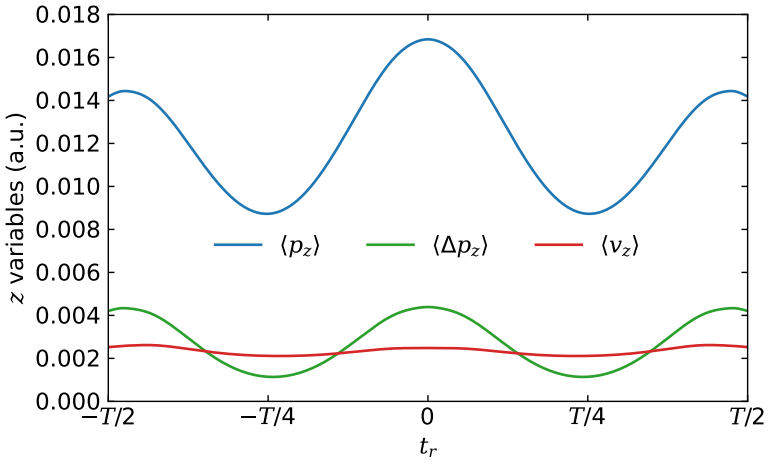

FIG. S1. Different contributions to the nonadiabatic modulation in linear momentum transfer for a sine-like pulse $\phi_{\mathrm{CEP}} = \pi/2$ calculated by ndSFA and SFA.

S4. ELLIPTICITY DEPENDENCE OF $\langle p_z\rangle$

The longitudinal momentum transfer $\langle p_z(\phi_p)\rangle$ features a characteristic dependence on the attoclock angle ϕ_p. However, the exact quantity is strongly dependent on the ellipticity of the ultrashort pulse. For ε well below $\varepsilon = 1$, $\langle p_z(\phi_p)\rangle$ features a pronounced minimum as discussed in the main text (Fig. S2). However, as $\varepsilon \to 1$ (circular polarization) the minimum becomes rapidly shallow and eventually turns into a shallow minimum determined by the pulse envelope.

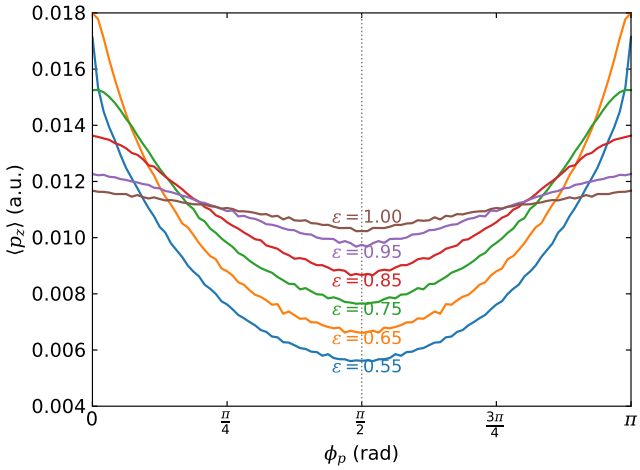

FIG. S2. Ellipticity dependence of $\langle p_z(\phi_p)\rangle$ for a cosine-like pulse $\phi_{\mathrm{CEP}} = 0$ calculated by ndSFA.

S5. WAVELENGTH SCALING OF $\langle p_z\rangle$

In order for the nondipole transfer of linear momentum to be detected more easily, performing attoclock experiments with midinfrared laser sources is a promising route. Here, we study the wavelength dependence of the final longitudinal momentum transfer while keeping the intensity fixed, as shown in Fig. S3. Clearly, as the wavelength increases, the nondipole effect gets larger and becomes more obvious [panel (a)]. Plotting the angle-integrated final linear momentum as a function of the wavelength, we find a quadratic increase of $\langle p_z\rangle$ with the wavelength [panel (b)] and the intercept is close to but not identical to $I_p/3c$, consistent with Eq. (5) of the main text.

The ionization probability peaks near but not exactly at the minimum of the linear momentum transfer, therefore

$$\langle p_z\rangle \gtrsim \frac{I_p}{3c} + \frac{\varepsilon^2 A_0^2}{2c} = \frac{I_p}{3c} + \frac{\varepsilon^2 F_0^2}{8\pi^2 c^3}\lambda^2. \tag{S37}$$

As a result, the slope is slightly larger than $\varepsilon^2 F_0^2/8\pi^2 c^3$, which is confirmed by our results.

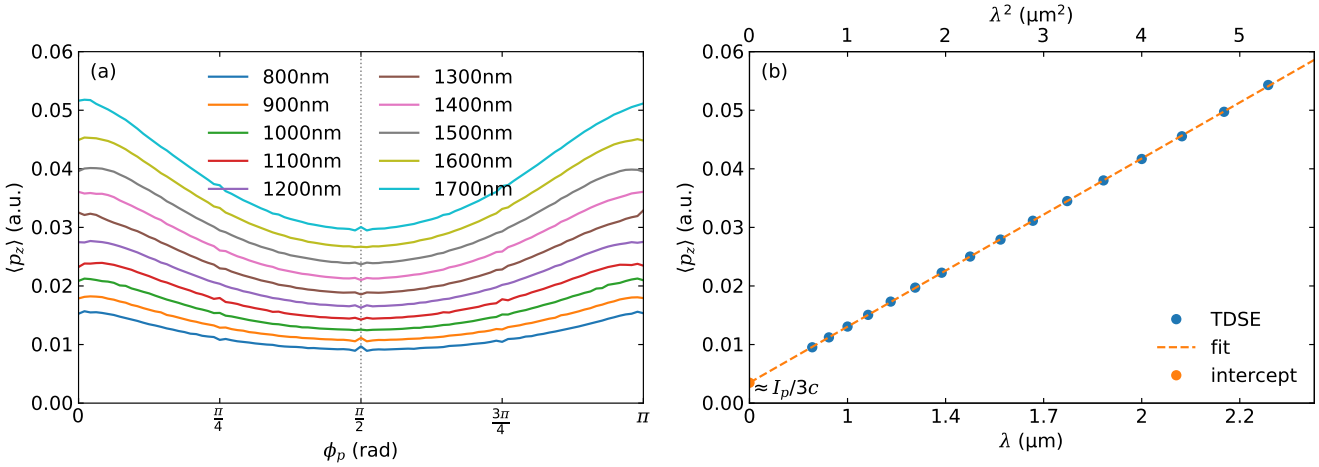

FIG. S3. Final longitudinal momentum for different laser wavelengths in (a) angle-resolved and (b) angle-integrated manner for a cosine-like pulse $\phi_{\mathrm{CEP}} = 0$ calculated by TDSE.

S6. INTENSITY AND DURATION DEPENDENCE OF $\langle v_z \rangle$

The intensity dependence of the linear momentum transfer at the tunnel exit $\langle v_z \rangle$ is shown in Fig. S4, featuring an intensity dependence of the linear momentum transfer at the tunnel exit. The modulation depth decreases as the laser intensity increases, because the Keldysh parameter decreases, meaning the tunneling becomes more adiabatic. The most important aspect here is that the modulation is in phase for different laser intensities, which ensures that such observation survives focal volume averaging.

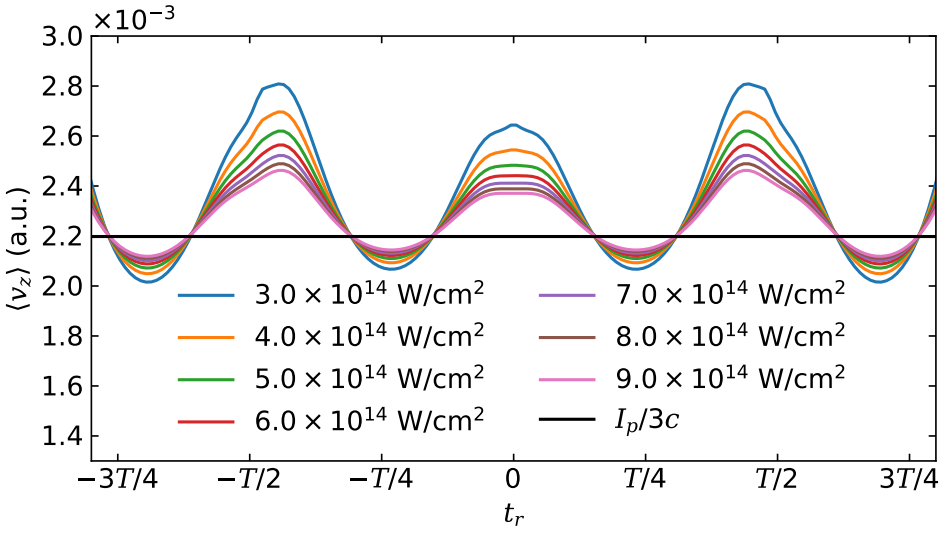

FIG. S4. Dependence of the linear momentum transfer $\langle v_z \rangle$ at the tunnel exit on the laser intensity for a sine-like pulse $\phi_{\mathrm{CEP}} = \pi/2$ calculated by ndSFA.

The length of the pulse is found not to be a critical parameter. The variation between different laser cycles results from their relative laser intensity (or field strength) within the respective time window. When the number of cycles increases for a given peak intensity, as shown in Fig. S5, the difference between different cycles decreases. Certainly, the modulation depth is larger for short pulses at both tails due to the lower intensity and larger Keldysh parameter. However, the ionization probability in the tails is low and does not contribute much to the main ionization peaks. Therefore, the exact pulse duration is not a critical parameter for an experimental verification of the nonadiabatic nondipole effect.

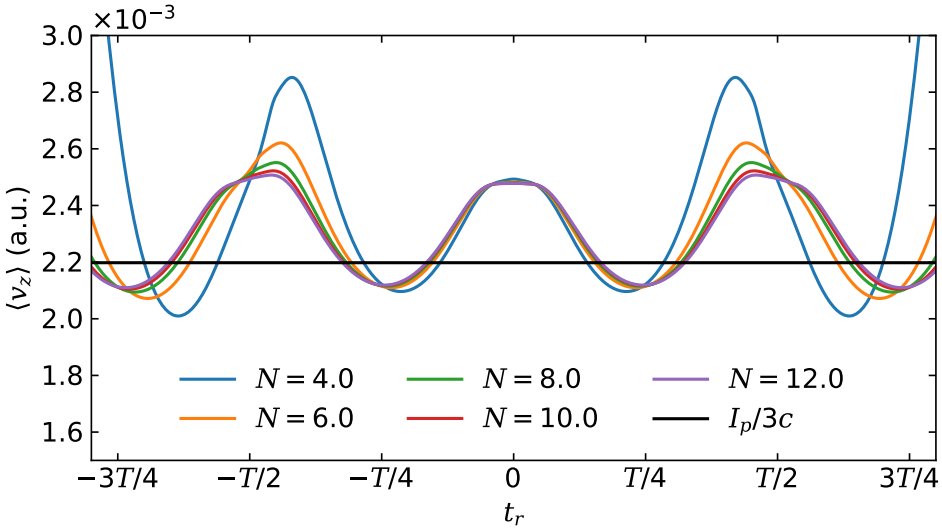

FIG. S5. Dependence of the linear momentum transfer $\langle v_z \rangle$ at the tunnel exit on the number of laser cycles for a sine-like pulse $\phi_{\mathrm{CEP}} = \pi/2$ calculated by ndSFA.

[1] H. Ni, U. Saalmann, and J. M. Rost, Phys. Rev. Lett. **117**, 023002 (2016).
[2] H. Ni, U. Saalmann, and J. M. Rost, Phys. Rev. A **97**, 013426 (2018).
[3] H. Ni, N. Eicke, C. Ruiz, J. Cai, F. Oppermann, N. I. Shvetsov-Shilovski, and L. W. Pi, Phys. Rev. A **98**, 013411 (2018).
[4] A. D. Bandrauk and H. Shen, J. Chem. Phys. **99**, 1185 (1993).
[5] X. M. Tong and S.-I. Chu, Chem. Phys. **217**, 119 (1997).
[6] X. M. Tong, J. Phys. B **50**, 144004 (2017).
[7] X. Gao, and X. M. Tong, Phys. Rev. A **100**, 063424 (2019).
[8] X. M. Tong, K. Hino, and N. Toshima, Phys. Rev. A **74**, 031405(R) (2006).
[9] G. F. Gribakin and M. Y. Kuchiev, Phys. Rev. A **55**, 3760 (1997).
[10] T. K. Kjeldsen and L. B. Madsen, Phys. Rev. A **74**, 023407 (2006).
[11] D. B. Milošević, G. G. Paulus, D. Bauer, and W. Becker, J. Phys. B **39**, R203 (2006).
[12] N. J. Kylstra, R. M. Potvliege, and C. J. Joachain, J. Phys. B **34**, L55 (2001).
[13] S. P. Goreslavski and S. V. Popruzhenko, Sov. Phys. JETP **83**, 661 (1996).
[14] N. I. Shvetsov-Shilovski, S. V. Popruzhenko, and S. P. Goreslavski, Laser Phys. **13**, 1054 (2003).
[15] S. P. Goreslavski, G. G. Paulus, S. V. Popruzhenko, and N. I. Shvetsov-Shilovski, Phys. Rev. Lett. **93**, 233002 (2004).
[16] M. V. Frolov, N. L. Manakov, A. A. Minina, S. V. Popruzhenko, and A. F. Starace, Phys. Rev. A **96**, 023406 (2017).
[17] A. M. Perelomov, V. S. Popov, and M. V. Terent'ev, Sov. Phys. JETP **23**, 924 (1966).
[18] A. M. Perelomov, V. S. Popov, and M. V. Terent'ev, Sov. Phys. JETP **24**, 207 (1967).
[19] A. M. Perelomov and V. S. Popov, Sov. Phys. JETP **25**, 336 (1967).
[20] V. D. Mur, S. V. Popruzhenko, and V. S. Popov, J. Exp. Theor. Phys. **92**, 777 (2001).
[21] V. S. Popov, Phys. Usp. **47**, 855 (2004).
[22] S. V. Popruzhenko, J. Phys. B **47**, 204001 (2014).
[23] B. M. Karnakov, V. D. Mur, S. V. Popruzhenko, and V. S. Popov, Phys. Usp. **58**, 3 (2015).
[24] B. Willenberg, J. Maurer, B. W. Mayer, and U. Keller, Nat. Commun. **10**, 5548 (2019).